

Electronic Raman scattering in quantum dots revisited

Alain Delgado^a, Augusto Gonzalez^b, and D.J. Lockwood^c *

^a *Centro de Aplicaciones Tecnológicas y Desarrollo Nuclear,
Calle 30 No 502, Miramar, Ciudad Habana, C.P. 11300, Cuba*

^b *Instituto de Cibernética, Matemática y Física, Calle E 309, Vedado, Ciudad Habana, Cuba*

^c *Institute for Microstructural Sciences, National Research Council, Ottawa, Canada K1A 0R6*

We present theoretical results concerning inelastic light (Raman) scattering from semiconductor quantum dots. The characteristics of each dot state (whether it is a collective or single-particle excitation, its multipolarity, and its spin) are determined independently of the Raman spectrum, in such a way that common beliefs used for level assignments in experimental spectra can be tested. We explore the usefulness of below band gap excitation and an external magnetic field to identify charge and spin excited states of a collective or single-particle nature.

PACS numbers: 78.30.Fs, 78.67.Hc, 78.20.Ls, 78.66.Fd

Keywords: A. Nanostructures; A. Semiconductors; D. Optical properties; E. Inelastic light scattering

I. INTRODUCTION

Raman scattering in semiconductor structures was devised more than twenty years ago by Burstein et. al. as a powerful tool for the identification of electronic excitations¹. To the best of our knowledge, experiments on Raman scattering in quantum dots were performed mainly before 1998.^{2,3,4} The lack of theoretical calculations for the relatively large dots used in the experiments (dozens of electrons per dot) made the experimental results less conclusive.

A second handicap of the experiments reported in Refs. [2,3,4] is related to the fact that they explored the conceptually difficult resonant regime, where the incident photon energy is in resonance with an electronic state in the conduction band. In contrast, the existing (qualitative) theory of Raman scattering is expected to be valid only well away from resonance⁵. It is usually called the off resonance approximation (ORA), and is well known for missing out the single-particle peaks in the Raman spectrum⁶, which are particularly important in the resonant regime. In Ref. [3], laser excitation energies 40 meV above band gap were used to identify collective states. The physics of Raman scattering under these conditions is expected to be still more complex because of the sudden increase of level widths with the opening up of the channel for spontaneous emission of longitudinal optical (LO) phonons⁷. The positions of collective peaks were computed by means of the ORA⁸, which constitutes a nice example of how one can get reasonable results with a theory that does not work in this regime.

In the present paper, we review a set of theoretical results on Raman scattering in relatively large quantum dots^{9,10,11,12}, which were motivated by the experiments described in Refs. [2,3,4].

We explore the below band gap excitation regime to study how the ORA is reached. In addition, it is shown

that this regime is ideal for the identification of the collective peaks and certain single-particle excitations (SPEs). Polarization rules for collective states, following from the ORA, are tested. They are unexpectedly shown to work also for the SPEs at zero magnetic field, and to break down in the presence of a field. Jump rules for the Raman peak intensities when the laser excitation energy approaches the band gap are also demonstrated.

Raman spectra computed with resonant excitation (but with the laser energy below the threshold for the creation of LO phonons) show extreme sensitivity to the excitation energy, and a reinforcement of single-particle peaks.

We hope that our detailed findings will motivate more experimental work on the Raman spectroscopy of quantum dots, which is regaining interest as a tool for studying small (with less than 7 electrons) self-assembled dots¹³.

II. GENERALITIES

A. The experimentalist point of view

A typical experimental setup for Raman measurements is sketched in Fig. 1. Usually, linear light polarization is used, although circular polarization would be very convenient in certain situations. We take the incident electric field to be in the plane of the dot, which is assumed quasi two-dimensional.

The backscattering geometry, in which the incident and scattered light beams go through the same optical fiber ($\phi_i = \phi_f$), is also very common.

Two kinds of measurements are usually performed in order to separate charge and spin excitations. In the so called polarized spectrum, (a), the final and incident electric fields are parallel, $\vec{E}_i \parallel \vec{E}_f$. Whereas the depolarized spectrum is taken with $\vec{E}_i \perp \vec{E}_f$, (b). Notice that oblique incidence ($\phi_i, \phi_f \neq 0$) is used to excite multipole final states.

*Corresponding author. email: David.Lockwood@nrc-cnrc.gc.ca

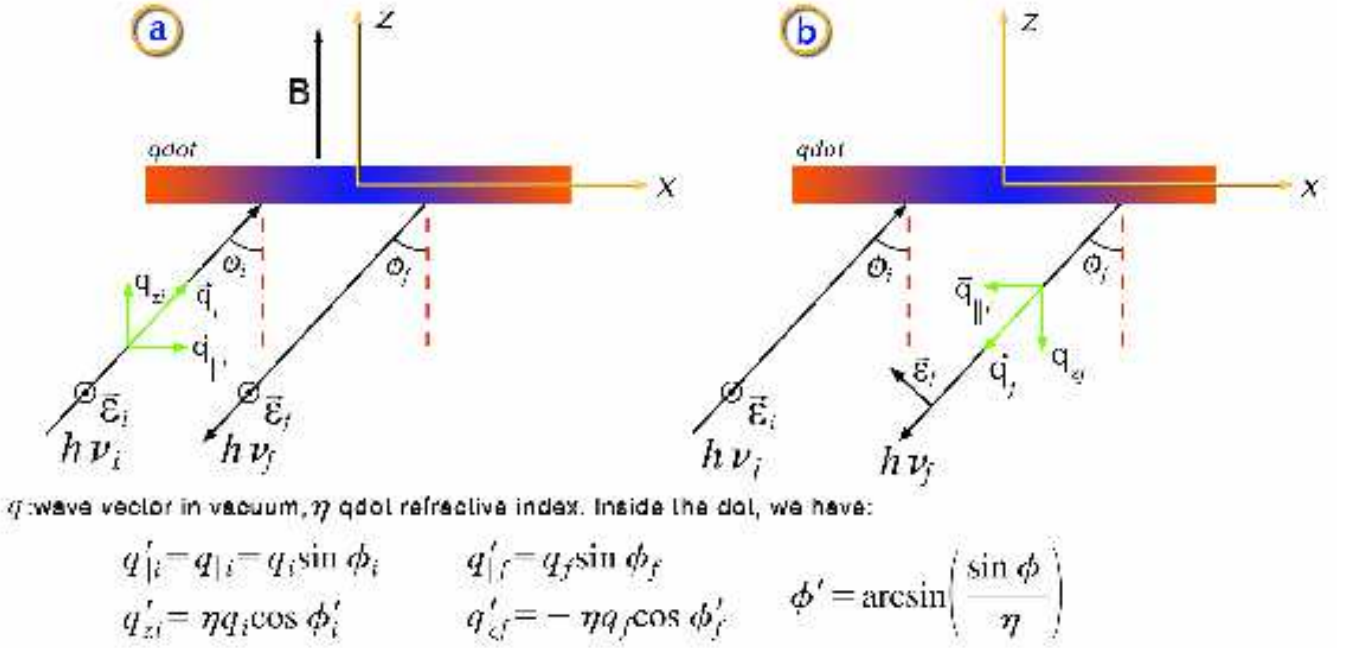


FIG. 1: Geometry of the Raman experiment: (a) polarized, and (b) depolarized geometry.

B. The theorist point of view

The theoretical representation of a Raman process emerges from the second-order perturbative result for the transition amplitude¹⁴, A_{fi} :

$$A_{fi} \sim \sum_{int} \frac{\langle f | H_{e-r}^+ | int \rangle \langle int | H_{e-r}^- | i \rangle}{h\nu_i - (E_{int} - E_i) + i\Gamma_{int}}. \quad (1)$$

A schematic representation is given in Fig. 2. The Raman scattering process can be viewed as the result of virtual transitions via all possible intermediate states. In the experiments, the incident photon energy, $h\nu_i$, is close to the effective band gap, so that we can restrict the sum to intermediate states that contain an additional electron-hole pair.

In the experiments, the temperature, T , is usually below 2 K. We present calculations at exactly $T = 0$ K, in which only the ground state of the N -electron quantum dot is initially populated. This will be our initial state, $|i\rangle$.

The intermediate electronic states, $|int\rangle$, as mentioned above, are states with an additional electron-hole pair. This pair is (virtually) recombined leading to a photon with energy $h\nu_f$. The electronic system ends up in a final state, $|f\rangle$. The energy difference, $\Delta E_f = E_f - E_i$, is the Raman shift. Notice the width, Γ_{int} , entering the expression for the transition amplitude in Eq. (1). We will consider intermediate states in an energy window of 30 meV above the band gap in order to neglect abrupt variations of Γ_{int} due to LO phonons. Γ_{int} will be fixed phe-

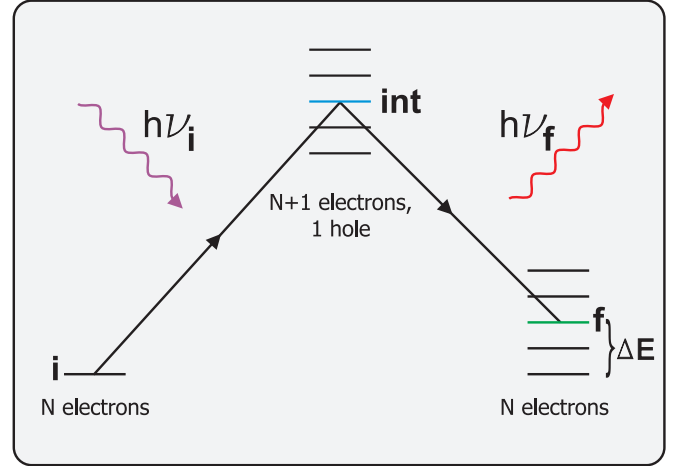


FIG. 2: The quantum mechanical transition amplitude and its interpretation in terms of virtual transitions.

nomenologically to a constant value, equal to 0.5 meV, which is due mainly to pair recombination.

From the transition amplitude one computes the cross section:

$$d\sigma \sim \sum_f |A_{fi}|^2 \delta(E_i + h\nu_i - E_f - h\nu_f). \quad (2)$$

Notice the energy conservation forced by the delta function, which implies that the Raman shift is equal to the

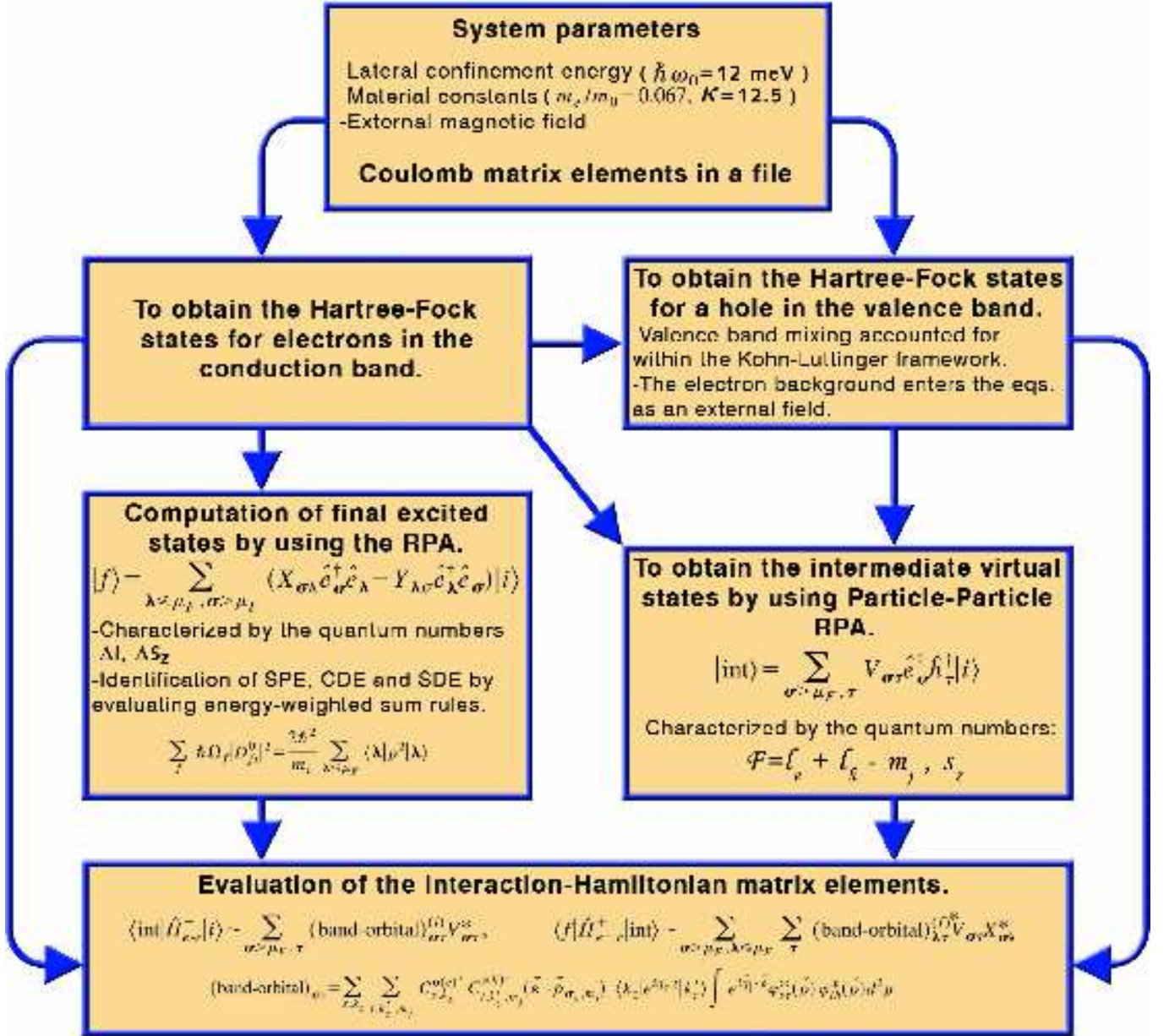


FIG. 3: The calculation scheme used in the paper.

photon energy loss. In our calculations, we replace the delta function by a Lorentzian:

$$\delta(x) \approx \frac{\Gamma_f/\pi}{x^2 + \Gamma_f^2}, \quad (3)$$

where the width of final states will also be assumed constant, $\Gamma_f = 0.1$ meV. A 30 meV excitation window for final states will be used in order to avoid considering phonon processes.

C. Calculation machinery

The calculation scheme, explicit expressions, and explanations can be found by the interested reader in papers [10,15]. We shall give in this section an overview of the conceptual and numerical procedure with the aid of Fig. 3.

The dot is modelled by a quantum well with hard walls in the z direction (the growth direction of the heterostructure), and a soft harmonic confinement ($\hbar\omega_0 = 12$ meV) in the x, y plane. The basis functions used to describe one-particle states in the dot are constructed as products of harmonic oscillator, infinite well, and spin

functions.

To save time in the calculation of many-electron wavefunctions, we computed the matrix elements of Coulomb interactions, $\langle \alpha, \beta | 1/r | \gamma, \delta \rangle$, where $\alpha, \beta, \gamma, \delta$ are arbitrary one-particle states, and stored them in a computer file. This calculation takes around 7 days in a personal computer. The matrix elements are loaded into the computer at the beginning of a calculation, allowing us to solve the nonlinear integro-differential Hartree-Fock (HF) equations for 42 electrons in a few minutes, or to compute all of the intermediate states entering a Raman process (around 10 000) in a few days. The HF equations for holes include the electrostatic field created by the background electrons in the dot, and take account of valence band mixing effects, as described by the Kohn-Luttinger Hamiltonian¹⁶. Up to 6 quantum-well sub-bands are considered in the HF equations for holes.

The final states of the Raman process are excited states of the N -electron system. The intermediate states, on the other hand, are states with $N + 1$ electrons and one hole. Both kinds of states are computed by means of random-phase-approximation (RPA) like ansatzs for the wavefunctions¹⁷, as illustrated in Fig. 3. It was already mentioned elsewhere¹⁰ that, in our opinion, the main limitation of using these functions in the present context is not related to the well-known lack of correlation effects in the RPA, but to the incomplete description of the density of energy levels in intermediate and final states.

Final states are labelled by the quantum numbers ΔL and ΔS_z , which refer to changes (with respect to the ground state) in the total angular momentum and total spin projections along the z axis. Borrowing a terminology from Nuclear Physics, we speak about monopole excitations when $\Delta L = 0$, dipole excitations when $\Delta L = \pm 1$, and quadrupole excitations when $\Delta L = \pm 2$. States are further classified by the degree of collectivity, computed with the help of energy-weighted sum rules¹⁷. For charge monopole excitations, for example, we have:

$$\sum_f \Delta E_f |D_{fi}^0|^2 = \frac{2\hbar^2}{m_e} \sum_{\lambda \leq \mu_F} \langle \lambda | \rho^2 | \lambda \rangle. \quad (4)$$

The left hand side of this equation contains only many-particle magnitudes, i.e., the excitation energies and the matrix elements of the monopole operator between the initial and final states, D_{fi}^0 (its explicit definition can be found in Ref. 15). The right hand side, however, can be evaluated in terms of the occupied HF orbitals, λ . The magnitude ρ is the cylindrical coordinate in the plane. We will conventionally say that the final state f is a collective state if $\Delta E_f |D_{fi}^0|^2$ is greater than 5% of the right hand side of Eq. (4). The same statement applies for other multipole excitations.

Concerning the spin quantum numbers, the formalism leads to ladders of final states characterized by ΔS_z . In

order to discriminate between different total spin states within a single ladder, we compare the energy differences of states in adjacent ladders with the corresponding Zeeman splitting. We talk about charge excitations above the ground state when the total spin does not vary, $\Delta S = 0$, and spin excitations when $\Delta S = \pm 1$. The distinction between collective and single-particle states is done on the basis of energy-weighted sum rules, which can be written for any multipolarity and ΔS . Collective excited states with $\Delta S = 0$ are called charge density excitations (CDEs), whilst collective states with $\Delta S = \pm 1$ are called spin density excitations (SDEs). The single-particle excitations are further distinguished by their charge or spin nature. Thus, we will refer to them as SPE(C) or SPE(S).

The intermediate states, on the other hand, are characterized by the spin S_z of the added electron, and the total pair angular momentum, $\mathcal{F} = l_e + l_h - m_j$.

Once the intermediate and final states of a Raman process are computed, the matrix elements of the electron-radiation interaction Hamiltonian are evaluated in terms of the coefficients entering the ansatz for the many-particle wavefunctions and the coefficients of the HF expansion. A complete Raman calculation, which requires the sum over all the intermediate and final states (previously stored into the computer), takes around one day in a personal computer.

D. The ORA

The ORA is a limit in which the expression for the amplitude of a Raman process is simplified. In this limit, only the initial and final state wavefunctions enter the expression for A_{fi} . The sum over intermediate states disappears from it. This means that, within the ORA, one can not explain phenomena such as intermediate state resonances in Raman processes.

The explicit derivation of the ORA for Raman scattering in quantum dots can be found in Ref. [11]. The assumptions for its derivation are basically two: (i) The laser excitation energy is far away from any intermediate state energy, in such a way that we can neglect the dependence of the denominator of Eq. (1) on E_{int} , and (ii) There is an energy window in the intermediate states (from E_{gap} to approximately $E_{gap} + 40$ meV) where the variations of Γ_{int} can be neglected and the completeness relation is practically fulfilled: $\sum'_{int} |int\rangle \langle int| \approx 1$. Under these assumptions, one can write:

$$A_{fi}^{ORA} \sim \langle f | H_{e-r}^+ H_{e-r}^- | i \rangle. \quad (5)$$

Using the explicit expression for H_{e-r} , one arrives at the ORA formula:

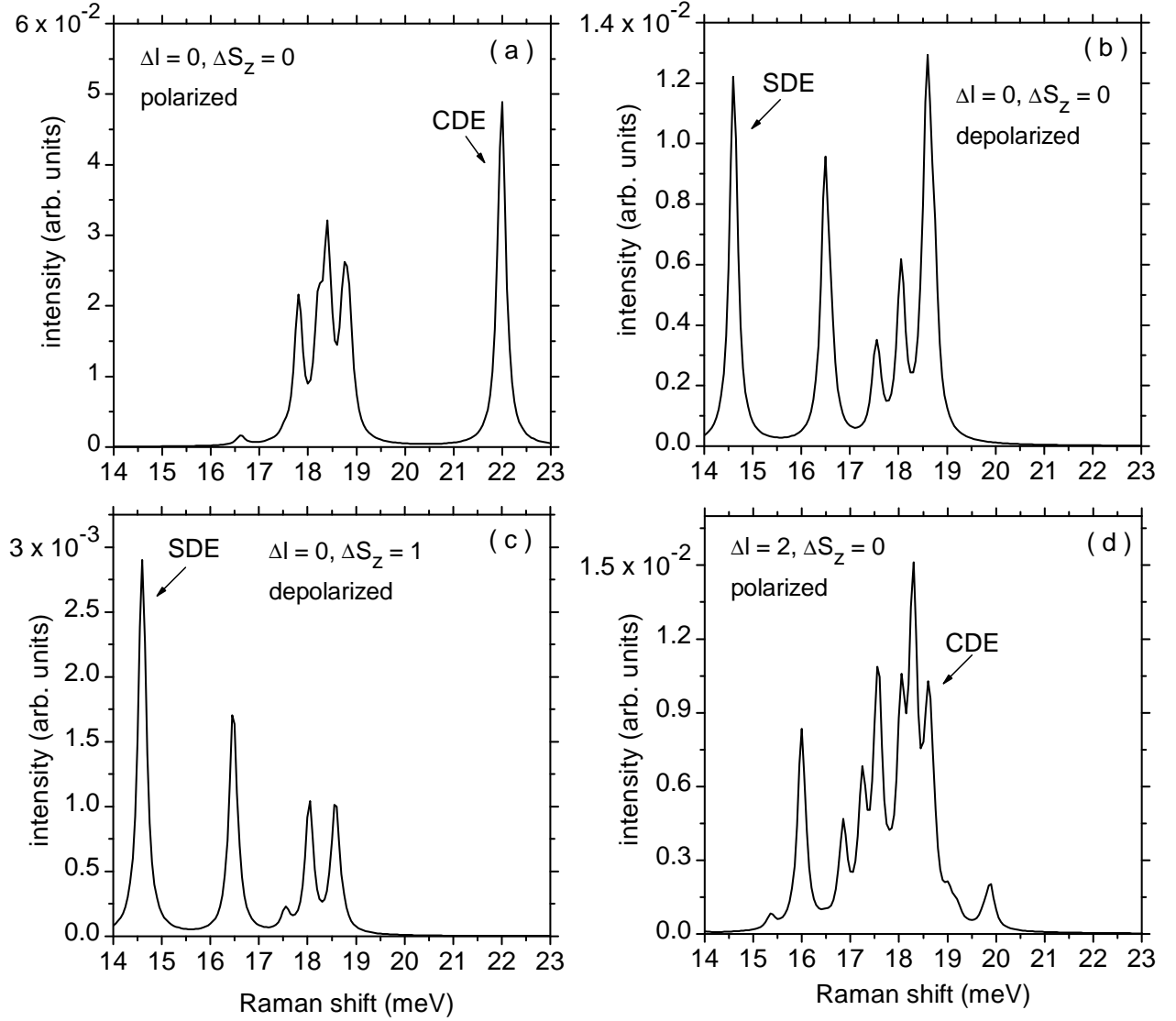


FIG. 4: Calculated Raman spectra in different channels. The incident laser energy is $h\nu_i = E_{gap} - 5$ meV.

$$\begin{aligned}
 A_{fi}^{ORA} \sim \sum_{\alpha, \alpha'} \langle \alpha | e^{i(\vec{q}_i - \vec{q}_f) \cdot \vec{r}} | \alpha' \rangle \left\{ \frac{2}{3} (\vec{\varepsilon}_i \cdot \vec{\varepsilon}_f) \langle f | e_{\alpha\uparrow}^\dagger e_{\alpha'\uparrow} + e_{\alpha\downarrow}^\dagger e_{\alpha'\downarrow} | i \rangle \right. \\
 \left. + \frac{i}{3} (\vec{\varepsilon}_i \times \vec{\varepsilon}_f) \cdot \langle f | \hat{z} (e_{\alpha\uparrow}^\dagger e_{\alpha'\uparrow} - e_{\alpha\downarrow}^\dagger e_{\alpha'\downarrow}) + (\hat{x} + i\hat{y}) e_{\alpha\uparrow}^\dagger e_{\alpha'\downarrow} + (\hat{x} - i\hat{y}) e_{\alpha\downarrow}^\dagger e_{\alpha'\uparrow} | i \rangle \right\}. \quad (6)
 \end{aligned}$$

A few important conclusions may be derived from Eq. (6). First, we notice that only collective final states have a nonvanishing amplitude in this approximation. The SPEs play no role in the Raman process. Indeed, by

expanding the exponential in Eq. (6), one can obtain an alternative expression for A_{fi}^{ORA} in terms of multipole operators¹⁵. Only final states having nonzero matrix elements of multipole operators will contribute to A_{fi}^{ORA} .

A second important conclusion is related to the spin selection rule for Raman scattering. Notice that, in Eq. (6), multipole operators that do not alter the spin quantum numbers of the initial state are multiplied by the factor $\vec{\epsilon}_i \cdot \vec{\epsilon}_f$. This means that peaks corresponding to charge operators will appear in the polarized geometry. On the other hand, multipole operators that modify the spin are multiplied by the factor $\vec{\epsilon}_i \times \vec{\epsilon}_f$ and, consequently, Raman peaks corresponding to spin excitations are expected to be seen in the depolarized geometry.

III. RESULTS

In the next two subsections, we present results for Raman intensities in quantum dots for laser excitation energies below and above band gap. In the former case, no experimental measurements have been performed so far. We expect weak Raman signals in this regime, but there are also many advantages such as, for example, the absence of a luminescence background, a smooth dependence of peak intensities on the excitation energy, etc¹⁰. On the other hand, in the above band gap excitation regime, our calculations are performed for an excitation window ranging from E_{gap} to $E_{gap} + 30$ meV, where E_{gap} is the effective quantum dot band gap. This is sometimes called the extreme resonance region.

A. Raman spectra with below band gap excitation

The salient features of the Raman spectra in this excitation regime are summarized below.

1. Dominance of monopole peaks

There are two reasons for the final state monopole excitations to be the dominant peaks in the Raman spectrum. First, Raman scattering proceeds via the (virtual) exchange of two photons. Selection rules dictate that the variation of the angular momentum (with respect to the initial state) should be preferably $\Delta L = 0, \pm 2$, etc. Second, the band-orbital factor in the matrix elements of H_{e-r} (see Fig. 3) provides roughly a factor $(qr)^l$ every time a pair is created or annihilated with a pair angular momentum l . As quantum dot dimensions are typically $r \sim 100$ nm,^{2,3} and the laser wavelength is $\lambda \sim 700$ nm, pairs with $l = 0$ dominate the process.

On the other hand, final state spin excitations in which there is a spin flip with respect to the initial state are depressed, as discussed elsewhere¹⁰. The Raman amplitude turns out to be proportional to the minority component of the Kohn-Luttinger hole wavefunction. This means that monopole spin excitations in which $\Delta S_z = 0$ should be the dominant peaks in the depolarized geometry.

We show in Fig. 4 some spectra in different angular momentum and spin channels for the purpose of com-

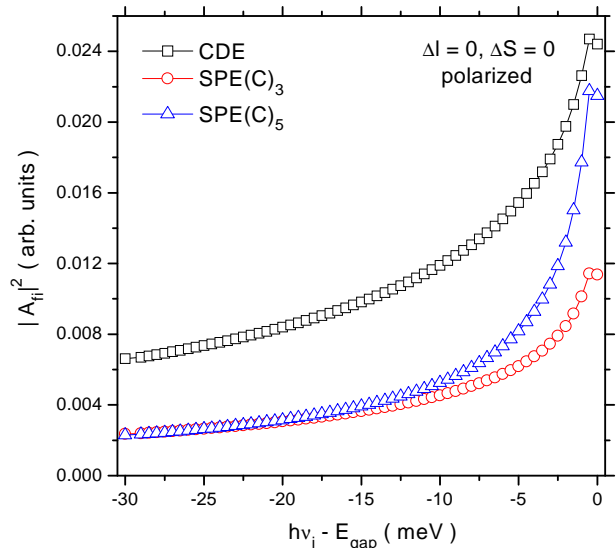


FIG. 5: $|A_{fi}|^2$ for the monopolar CDE and two SPEs(C) with excitation energies 17.8 and 18.4 meV, respectively.

parison. The laser energy is 5 meV below the band gap, and the incident (and backscattered) angle is equal to 20°. Charge monopolar, charge quadrupolar, and spin monopolar peaks (with no spin flips) exhibit comparable magnitudes. Dipolar (not shown) or spin-flip excitations lead to Raman peak intensities one or two orders of magnitude lower than charge monopolar peaks.

2. Smooth dependence of peak intensities on the excitation energy

The intensities of individual Raman peaks show a smooth dependence on $h\nu_i$ when the latter is below the band gap. This is simply understood from the Eq. (1) for the transition amplitude. From the experimental point of view, it is a nice feature. The identification of individual peaks could not be easier.

According to the ORA, as $h\nu_i$ moves away from the band gap, the collective states should start dominating the Raman spectrum. In this way, we can identify the collective and single-particle excitations (mainly the monopolar and quadrupolar ones) by varying $h\nu_i$. We show in Fig. 5 the amplitude squared, $|A_{fi}|^2$, computed in the polarized geometry, for three charge monopolar final states. One of them is the CDE, and the other two are SPEs with excitation energies 17.8 and 18.4 meV, respectively. The CDE already becomes the dominant peak when $h\nu_i$ is around 3 meV below the band gap.

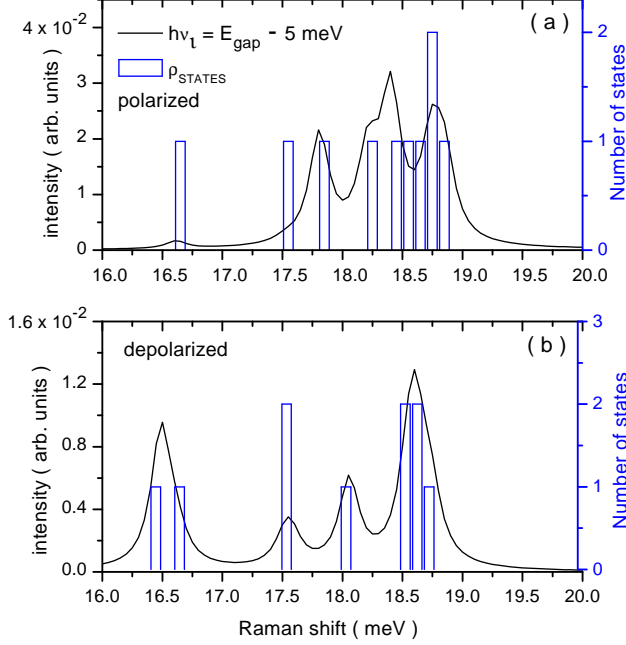


FIG. 6: Polarized and depolarized monopolar Raman spectra and their comparison with the density of final state SPEs.

3. Correlation between the SPE Raman peaks and the density of final state energy levels

It is natural to expect Raman peaks to be located there where there is an agglomeration of final states². In this paragraph, we take a step further and compare the polarized Raman spectrum with the density of final state SPEs(C), and the depolarized spectrum with the density of SPEs(S). This is an attempt to test the spin selection rules, derived from the ORA for the collective excitations, in the SPEs.

The comparison is given in Fig. 6, where we show results in the monopolar channel. Unexpectedly, the correlation is high, particularly in the depolarized geometry. It is instructive to comment on a commonly held belief that the SPEs appear in both polarized and depolarized spectra. Of course, it is true. But it would be better to say that the SPEs(C) appear mainly in the polarized geometry, and the SPEs(S) mainly in the depolarized geometry. This statement is valid at zero magnetic field.

4. Breakdown of the polarization selection rules in a magnetic field

In a magnetic field, the selection rules deduced from the ORA for the collective states are no longer valid at excitation energies close to the band gap. The reason is the magnetic field dependence of energies and wave-

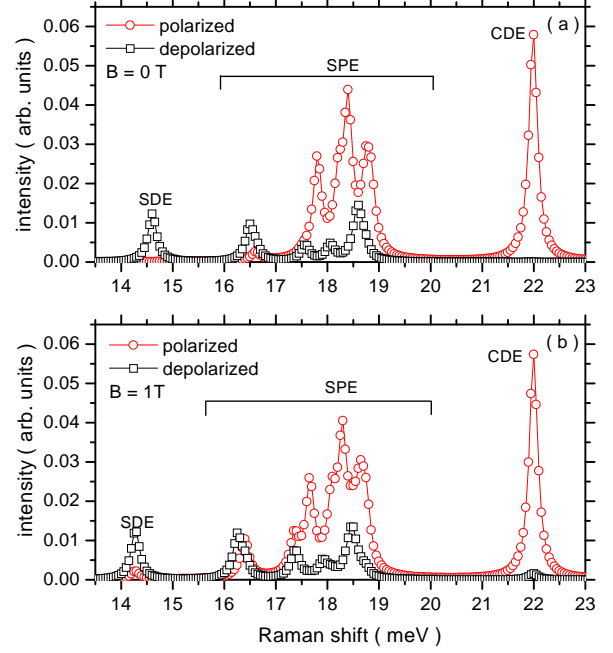


FIG. 7: Polarized and depolarized monopolar Raman spectra at $B = 0$ and 1 T.

functions of intermediate states entering the summation of Eq. (1). The situation is depicted in Fig. 7, where monopolar Raman spectra at $B = 0$ and 1 T are drawn. The excitation energy is $h\nu_i = E_{\text{gap}} - 2.5$ meV.

Let us define the polarization ratio of a single final state, $|f\rangle$, as the ratio of $|A_{fi}|^2$ in unfavorable and favorable geometries, i.e., $r = |A_{fi}(\text{unfavorable})|^2 / |A_{fi}(\text{favorable})|^2$. By favorable we mean the polarized geometry for a charge excitation, and the depolarized geometry for a spin excitation.

The polarization ratios for the collective states at $B = 0$ are 3×10^{-4} for the CDE, and 2×10^{-7} for the SDE. That is, an almost perfect fulfillment of the ORA selection rules in spite of the fact that $h\nu_i$ is only 2.5 meV below band gap. At $B = 1$ T, however, these numbers change to 0.03 and 0.17, respectively.

The fulfillment of the selection rules for the SPEs is not so evident in Fig. 7, because these states, with excitation energies between 16 and 19 meV, are not as easily distinguishable as the collective ones. From the data used to draw this figure, we can compute r for each SPE. The average polarization ratios at $B = 0$ are 3×10^{-3} for the SPEs(C), and 2×10^{-4} for the SPEs(S). At $B = 1$ T, these numbers become 0.26 and 1.1, respectively. That is, the intensities in both geometries become comparable.

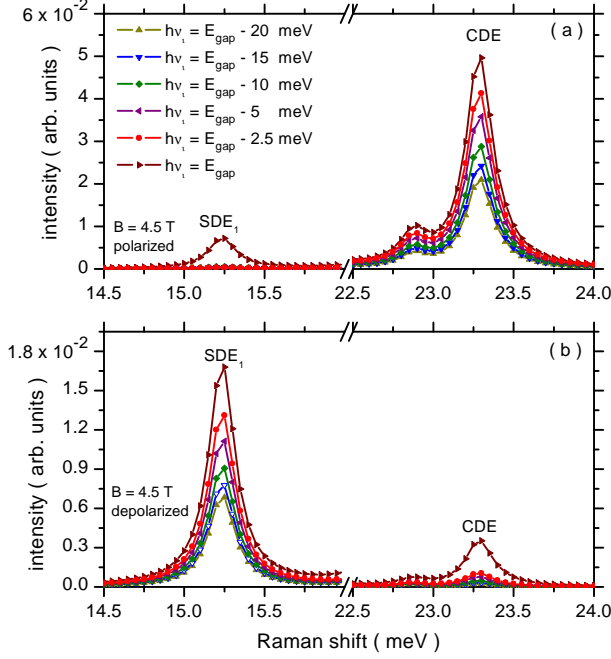


FIG. 8: Polarized and depolarized monopolar Raman spectra at $B = 4.5$ T as $h\nu_i$ approaches the band gap.

5. Jump rule at the band gap

Near the band gap, the intensities of Raman peaks follow an interesting behavior. Let us focus on the collective excitations and compare the intensities of the CDE and SDE peaks as a function of $h\nu_i$. The results for the monopolar spectra at $B = 4.5$ T are shown in Fig. 8.

We observe a smooth increase of peak intensity in the favorable geometry as $h\nu_i$ approaches the band gap. In the unfavorable geometry, however, the intensity remains practically constant up to the moment when $h\nu_i$ reaches the band gap, where there is a sudden variation. We call this phenomenon the “jump rule”. SPEs also largely follow this rule.

B. Raman spectra under resonant excitation

We return now to the $B = 0$ case, and increase the laser energy to values above the band gap. As mentioned above, we restrict $h\nu_i$ to the interval $(E_{\text{gap}}, E_{\text{gap}} + 30 \text{ meV})$ in order to avoid considering phonon effects.

Many of the properties discussed in the preceding section are still valid in the present context. For example, the monopolar and quadrupolar peaks are the most important peaks in the Raman spectrum, and the density of final state energy levels is correlated with the positions of the principal Raman lines.

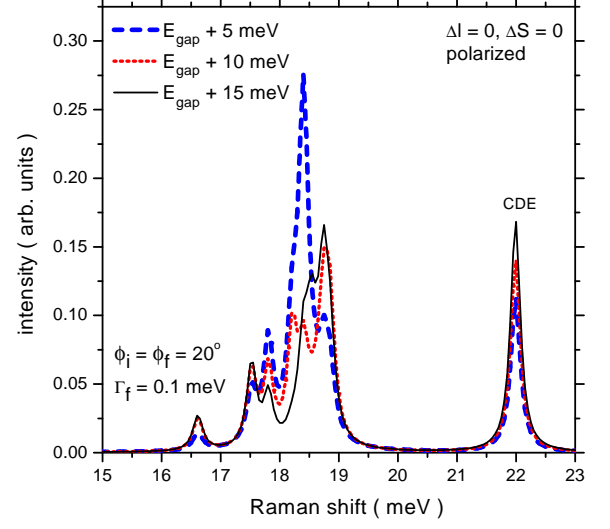


FIG. 9: Monopolar Raman spectra above band gap in the polarized geometry.

In addition, there are certain new features, which characterize the resonant excitation regime.

1. Dominance of SPEs

Raman peaks related to SPEs experience a noticeable increase of intensity under resonant excitation. Qualitatively speaking, one can say that Raman scattering proceeds through a single intermediate state (the one exactly at resonance), which (virtually) decays indiscriminately to the collective final state or to the SPEs. As there is a large number of SPEs, and they are packed in groups, the intensities of the corresponding peaks can be high.

This statement is illustrated in Fig. 9, where three spectra corresponding to $h\nu_i = E_{\text{gap}} + 5 \text{ meV}$, $E_{\text{gap}} + 10 \text{ meV}$, and $E_{\text{gap}} + 15 \text{ meV}$, respectively, are shown. In addition, we observe a non-monotonous dependence of peak intensities on $h\nu_i$. This is a consequence of the fact that, when $h\nu_i$ is varied, a different intermediate state comes into resonance.

2. Correlation between the Raman intensities of individual states and the density of intermediate state energy levels

Here, we show how by monitoring the intensities of individual peaks as a function of $h\nu_i$ one can obtain information about the density of energy levels in intermediate states, at least at low excitation energies above the band gap.

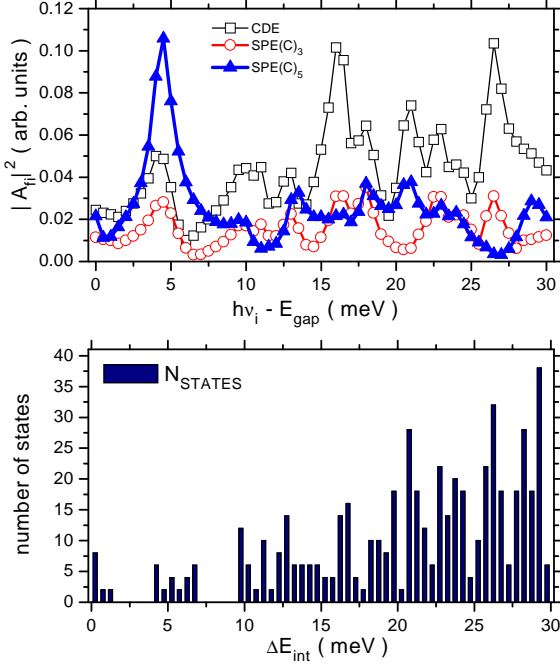


FIG. 10: Upper panel: $|A_{fi}|^2$ for the same three charge monopolar states used in Fig. 5 and $h\nu_i$ above band gap. Lower panel: Histogram of intermediate state energy levels.

In Fig. 10, we follow the same final states used in Fig. 5, and compare the corresponding $|A_{fi}|^2$ for $h\nu_i$ in the interval $(E_{gap}, E_{gap} + 30 \text{ meV})$ with the density of energy levels.

The first peak of $|A_{fi}|^2$ near 5 meV above the band gap signals the beginning of a group of energy levels. A second structure is seen near 10 meV above the band gap, where there is also a threshold. At higher excitation energies there is still some correlation between peaks in $|A_{fi}|^2$ and peaks in the density of intermediate state energy levels.

3. Absence of interference effects

We now evaluate the contribution of the different intermediate states entering the summation of Eq. (1) in resonant Raman scattering. The postulate is that the qualitative picture sketched in Sec. IIIB1 is correct: only those intermediate states whose energies are very close to $h\nu_i$ contribute to the Raman amplitude. To verify this, we performed different calculations of A_{fi} , restricting the sum over intermediate states to the window $(h\nu_i - \delta E, h\nu_i + \delta E)$. There is qualitatively no change in the spectrum when δE is reduced from 10 down to 2 meV.

We compare in Fig. 11 the magnitude $|A_{fi}|^2$ for the spin monopolar peak with $\Delta E_f = 18 \text{ meV}$ with the individual contributions of each intermediate state to the

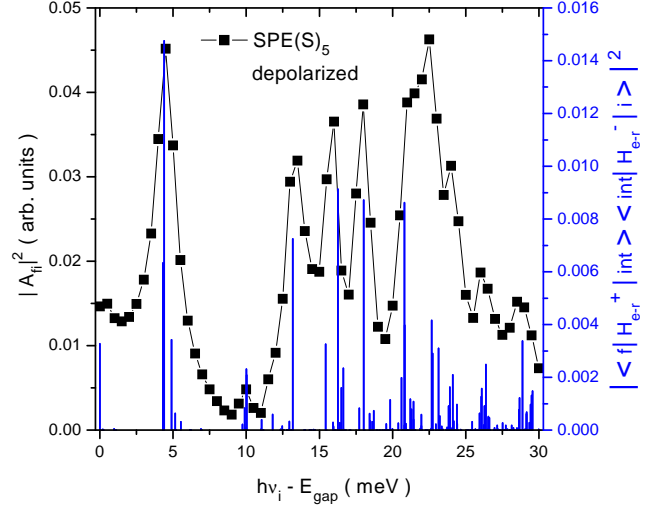


FIG. 11: $|A_{fi}|^2$ for the spin monopolar state with excitation energy $\Delta E_f = 18 \text{ meV}$ and the contribution of each individual intermediate state to the sum.

sum. No strong cancellation effects nor strong cooperation effects are apparent. That is, interference effects in A_{fi} are weak under resonant excitation.

4. Selection rules in a magnetic field

The polarization selection rules that follow from the ORA may be tested for excitation energies above the band gap. Surprisingly, they shown to be very well obeyed at zero magnetic field, and break down in a magnetic field. The polarization ratio exhibits a strong dependence on $h\nu_i$ and on the applied field. In quality of example, let us consider the monopole SDE. At zero field, r is practically zero (10^{-7} when $h\nu_i = E_{gap} + 5 \text{ meV}$). But at $B = 1 \text{ T}$, r varies from 1.1 at the band gap to 0.1 for $h\nu_i = E_{gap} + 2.5 \text{ meV}$.

IV. CONCLUSIONS

These theoretical calculations of the Raman spectrum of a many-electron quantum dot in zero and non zero applied magnetic field have revealed intriguing new features and a great sensitivity to the excitation energy.

For excitation energies below the band gap, we found Raman spectra dominated by the collective excitations already when $h\nu_i = E_{gap} - 5 \text{ meV}$. The peak intensities depend smoothly on the excitation energy. In zero field, the simple-minded polarization selection rules – CDE polarized/SDE depolarized – are very well obeyed even by the SPEs. This means that one can obtain information

about the density of final state SPEs from the Raman spectra. In an applied magnetic field, these basic selection rules break down, particularly when $\hbar\nu_i$ is increased up to the band gap, where the Raman intensities of the collective excitations in their “forbidden” geometries suddenly increase to appreciable values. This we termed the Raman intensity “jump rule”, and may help to determine the charge or spin character of a single excitation.

A quite different situation is encountered for excitation at energies above the band gap. The Raman peak intensities fluctuate considerably as the excitation energy sweeps through resonance with intermediate states. In this regime, the SPEs dominate the Raman spectrum, the Raman intensities of individual peaks correlate well

with the density of intermediate state energy levels, and there is an absence of interference effects.

It would be interesting now to explore experimentally these new features of the electronic Raman spectrum of many-electron quantum dots.

Acknowledgments

Part of this work was performed at the Institute for Microstructural Sciences (IMS), National Research Council, Ottawa. A.D. acknowledges the hospitality and support of IMS.

-
- ¹ E. Burstein, A. Pinczuk, and S. Buchner, in B.L.H. Wilson (ed.), *The Physics of Semiconductors*, Institute of Physics, Bristol, 1979.
 - ² D.J. Lockwood, P. Hawrylak, P.D. Wang, C.M. Sotomayor Torres, A. Pinczuk, and B.S. Dennis, *Phys. Rev. Lett.* **77** (1996) 354.
 - ³ C. Schuller, K. Keller, G. Biese, E. Ulrichs, L. Rolf, C. Steinebach, D. Heitmann, and K. Eberl, *Phys. Rev. Lett.* **80** (1998) 2673.
 - ⁴ C.M. Sotomayor-Torres, D.J. Lockwood, and P.D. Wang, *J. Electr. Materials* **29** (2000) 576.
 - ⁵ M. Cardona (ed.), *Light scattering in solids*, 2nd edition, Springer-Verlag, New-York, 1982.
 - ⁶ Daw-Wei Wang and S. Das Sarma, *Phys. Rev. B* **65** (2002) 125322.
 - ⁷ H. Htoon, D. Kulik, O. Baklenov, A.L. Holmes, Jr., T. Takagahara, and C.K. Shih, *Phys. Rev. B* **63** (2001) 241303.
 - ⁸ M. Barranco, L. Colletti, A. Emperador, E. Lipparini, M. Pi, and Ll. Serra, *Phys. Rev. B* **61** (2000) 8289.
 - ⁹ A. Delgado and A. Gonzalez, *J. Phys.: Condens. Matter* **15** (2003) 4259.
 - ¹⁰ A. Delgado, A. Gonzalez, and D.J. Lockwood, *Phys. Rev. B* **69** (2004) 155314.
 - ¹¹ A. Gonzalez and A. Delgado, <http://arxiv.org/cond-mat/0408510>, to appear in *Physica E*.
 - ¹² A. Delgado, A. Gonzalez, and D.J. Lockwood, to be submitted.
 - ¹³ T. Brocke, M.-T. Bootsmann, M. Tews, B. Wunsch, D. Pfannkuche, Ch. Heyn, W. Hansen, D. Heitmann, and C. Schuller, *Phys. Rev. Lett.* **91** (2003) 257401.
 - ¹⁴ R. Loudon, *Adv. Phys.* **13** (1964) 423.
 - ¹⁵ A. Delgado, A. Gonzalez and E. Menendez-Proupin, *Phys. Rev. B* **65** (2002) 155306.
 - ¹⁶ G. Bastard, *Wave mechanics applied to semiconductor heterostructures*, Les editions de physique, Les Ulis Cedex, 1998.
 - ¹⁷ P. Ring and P. Schuck, *The Nuclear Many-Body Problem*, Springer-Verlag, New-York, 1980.